Cancer Nanotechnology

RESEARCH Open Access

SiO_2–alginate–melittin nano-conjugates suppress the proliferation of ovarian cancer cells: a controlled release approach leveraging alginate lyase

Lihui Si[1], Shuli Yang[1], Ruixin Lin[2], Shiyu Gu[1], Chuhan Yan[1] and Jia Yan[1*]

*Correspondence:
jiayan@jlu.edu.cn

[1] Department of Gynecology and Obstetrics, The Second Hospital of Jilin University, No.218, Ziqiang Street, Nanguan District, Changchun 130041, Jilin, China
[2] Department of Hepatopancreatobiliary Surgery, The Second Hospital of Jilin University, Changchun 130041, China

Abstract

Background: Ovarian cancer treatment is challenged by resistance and off-target effects. Melittin shows promise against cancer but is limited by its instability and harmful cellular interactions. Our study introduces SiO2–alginate–melittin nano-conjugates (SAMNs), incorporating alginate lyase to enhance melittin's release and mitigate alginate drawbacks.

Methods: We combined melittin with alginate and mesoporous silica, using alginate lyase to control melittin release. Effects on SKOV3 ovarian cancer cells were evaluated via viability, invasion, migration assays, ROS levels, apoptosis-related proteins, and mitochondrial function tests.

Results: SAMNs extended melittin's cell control, reducing proliferation, invasion, and migration compared to free melittin. Alginate lyase facilitated controlled melittin release, decreasing off-target cytotoxicity. The only melittin group showed severe mitochondrial impairment, while the SAMNs and lyase groups had moderated impacts, indicating a dose-dependent effect on mitochondrial health and cell uptake.

Conclusions: SAMNs, especially with alginate lyase, offer an effective strategy for ovarian cancer treatment, optimizing melittin delivery while minimizing adverse effects of alginate. This approach enhances the therapeutic potential of melittin in combating ovarian cancer.

Keywords: Ovarian cancer, Melittin, Sio_2–alginate–melittin nano-conjugates, Apoptosis, Reactive oxygen species, Alginate lyase, Mitochondrial functions

Background

Ovarian cancer is one of the most lethal gynecologic malignancies, accounting for a substantial number of cancer-related deaths in women worldwide. The high mortality rate is primarily due to the late-stage diagnosis and the development of resistance to conventional chemotherapies and serious side effects (Bauersfeld et al. 2018; Kuroki & Guntupalli 2020; Pokhriyal et al. 2019). Therefore, the exploration of novel therapeutic

strategies is of paramount importance to improve the prognosis and survival rate of patients with ovarian cancer.

Peptides, as potential anticancer agents, have attracted considerable attention due to their high specificity, low toxicity, and ease of modification (Dai et al. 2020). Melittin, the principal component of bee venom, is one such peptide that has demonstrated potent anticancer activity across various cancer types, including ovarian cancer (Badr-Eldin et al. 2021). However, the clinical application of melittin is limited by its potential off-target cytotoxic effects and rapid degradation in the body (Akbari et al. 2022). To overcome these challenges, nanoparticle-based drug delivery systems have been extensively explored due to their ability to improve the stability, bioavailability, and targeted delivery of therapeutic agents (Akbarzadeh-Khiavi et al. 2022; Qi et al. 2019). Alginate, a natural polysaccharide extracted from brown seaweed, is an attractive material for nanoparticle synthesis owing to its biocompatibility, biodegradability, and ability to form nanoparticles through ionic gelation (Severino et al. 2019; Sorasitthiyanukarn et al. 2022).

Harnessing the power of innovative therapeutic delivery systems, the medical field has seen a surge in interest around the use of alginate nanoparticles in cancer prevention. These biocompatible, biodegradable, and nontoxic polymers are an ideal medium for safely transporting potent anti-cancer agents, such as melittin, directly to cancerous cells. Derived from bee venom, melittin has displayed significant anti-cancer potential, but its unregulated application can also harm healthy cells. By encapsulating melittin within alginate nanoparticles, we can ensure release at the target site, thereby mitigating potential collateral damage. The application of alginate lyase further optimizes this system, as this enzyme can digest the alginate nanoparticles (Keaswejjareansuk et al. 2021) and trigger the release of the encapsulated melittin. This ensures a gradual release, enabling sustained therapeutic activity against cancer cells while minimizing toxicity risks. The strategic combination of alginate nanoparticles, melittin, and alginate lyase presents a pioneering approach in our fight against cancer, promising safer and more effective treatment methods. SiO2–alginate shows promise as a carrier for various therapeutic agents targeting the ovarian cancer cell line SKOV-3 (Alizadeh et al. 2020). Although many studies have been performed with melittin in the prevention of numerous types of cancers (Badr-Eldin et al 2020; Mir Hassani et al. 2021; Sangboonruang et al. 2020; Zhou et al. 2021), SiO_2–alginate–melittin nano-conjugates (SAMNs) has not been well-defined in ovarian cancer yet. Addressing these issues, our study focuses on SiO2–alginate–melittin nano-conjugates (SAMNs), utilizing alginate as an encapsulating agent for melittin. Despite alginate's favorable properties, its slow degradation rate and tendency to release high molecular weight strands pose challenges in efficient body clearance and controlled melittin release (Datta et al. 2020). To overcome these limitations, we have incorporated alginate lyase into our formulation, aiming to expedite alginate degradation and ensure a more predictable melittin release.

Experimental section

Cell culture

The SKOV3 ovarian cancer cell line was procured from the Cell Bank of the Institute of Biological Science, CAS, Shanghai, China. Cultures were maintained in McCoy's 5a medium, fortified with 10% fetal bovine serum (FBS) and 100 μg/L

penicillin–streptomycin, obtained from Gibco, NY, USA. Cells were incubated under standardized conditions at 37 °C with a 5% CO_2 atmosphere.

Synthesis and analysis of melittin

Melittin, characterized by the sequence GIGAVLKVLTTGLPALISWIKRKRQQ (Akbari et al. 2022), was custom-synthesized by Harbin Jingwei Baike Biotechnology Co., Ltd, Harbin, China. The integrity and molecular weight of the peptide were validated through High-Performance Liquid Chromatography (HPLC, Agilent Technologies, CA, US) and Electrospray Ionization–Mass Spectrometry (ESI–MS, Thermo Fisher Scientific, MA, USA). To augment the ionization efficiency in ESI's negative ion mode, 15 µL of ammonia was supplemented to a 1 mL melittin solution. Parameters set for the analysis included an injection flow rate of 180 µL/h, polarization voltage of 3500 V, capillary inlet voltage of 4000 V, outlet voltage of 320 V, and a mass range between 150 and 3000 Da.

Synthesis and characterization of SAMN

Initially, 0.3 g of cetyltrimethylammonium bromide (CTAB) was dissolved in 60 mL of deionized water under magnetic stirring. Sequentially, 9 mL of ethylene glycol and 4 mL of ammonia were incorporated, followed by incubation at 50 °C for 15 min. Subsequently, 4 mL of tetraethyl orthosilicate (TEOS) was integrated, allowing the reaction to proceed for 3 h. The resultant blend was centrifuged, rinsed with deionized water, dried under vacuum at 60 °C, and then calcined at 550 °C for 3 h, ensuring complete removal of organic compounds. Aminated mesoporous silica was synthesized by mixing 0.3 g of the prepared silica in 60 mL of ethanol and 4 mL of deionized water. The solution was then heated to 48 °C under magnetic stirring, followed by the addition of 2.5 mL of 3-aminopropyltriethoxysilane (APTES). After a 24 h reaction, the product was centrifuged, rinsed, and dried under vacuum at 60 °C. 40 mg of aminated mesoporous silica was combined with 25 mL each of ethanol and deionized water, and the temperature was adjusted to 80 °C. Upon the addition of 120 mg of sodium 2-bromoethylsulfonate, the pH was modulated to the 8–9 range using a NaOH solution (1 mg/mL). After a 5 h reaction, the mixture was centrifuged, washed with ethanol, and vacuum-dried at 60 °C. Alginate (2 g, Sigma) was dissolved in 50 mL ddH_2O solution at 95 °C for 10 min and allowed to equilibrate at 22 °C for 2 h. Melittin powder was then added to 10 mL of this 2% alginate solution, establishing various melittin concentrations, with a melittin-free alginate solution serving as a control. A 10 mL aliquot of the alginate solution, either with or without melittin, was taken, and 20 mg of sulfonated mesoporous silica was dispersed within under magnetic stirring. This mixture was stirred at 4 °C for 12 h, then centrifuged and rinsed with deionized water. The combination of electrostatic adsorption and a porous structure enabled the loading of melittin and/or alginate into the silica. The resulting nano-conjugates were visualized using Scanning Electron Microscopy (SEM). Fourier-transform infrared spectroscopy (FTIR, PIKE Technologies, Inc., MA, USA) was employed to discern the absorption characteristics of SiO_2, alginate, melittin, and SAMN. Samples were cast in potassium bromide discs and analyzed in a consistent experimental environment. Spectra were generated across a range of 4000–500 cm^{-1} with a resolution of 4 cm^{-1}, utilizing 8 scans for optimal results. Dynamic Light Scattering (DLS) was employed to measure the size distribution of SiO_2 and SAMN

nanoparticles (Babick 2020). Ten mg of each nanoparticle type was weighed and suspended in 1 mL of PBS (pH 7.4). The measurements were conducted using the Malvern Zetasizer Nano ZS instrument (BeiYiTiao, Beijing, China).

Release kinetics of melittin

To determine the release kinetics of melittin from nanoparticles in the presence of alginate lyase, the following procedure was established. One hundred mg of melittin-loaded nanoparticles was first weighed out and then suspended in 1 mL of Phosphate-buffered saline (PBS, pH 7.4). To this suspension, 0.1, 0.5 and 1 μM of alginate lyase was added. The mixture was then incubated at 37 °C in a shaking incubator to ensure consistent exposure and mixing. At predetermined time intervals, 6, 12, 24, 48, 72 and 96 h, 100 μL aliquot was removed from the suspension. Each aliquot was centrifuged at 10,000 rpm for 10 min, ensuring the nanoparticles settled at the bottom. The supernatant, carefully separated without disturbing the nanoparticle pellet, was then analyzed using a high-performance liquid chromatography (HPLC) system to ascertain the melittin content. This HPLC system was calibrated and appropriately set for melittin detection. To assess the release kinetics of melittin in the presence of different concentrations of alginate lyase, we employed four distinct models, each with its specific parameters. Data were collected at regular time intervals (6, 24, 48, 72, 96 h) for varying concentrations of alginate lyase (0, 0.1, 0.5, 1 μM). Zero-Order Release assumes a constant release rate, independent of the drug concentration. For this, the average melittin release (in μg/mL) was plotted directly against time (in hours). In first-order release model, the rate of drug release is proportional to its remaining concentration. To visualize this, the natural logarithm of the average melittin release was plotted against time. Higuchi Model describes drug release from insoluble matrices based on Fickian diffusion. The average melittin release was plotted against the square root of time to achieve this representation. Korsmeyer–Peppas Model is generally applied to polymeric drug delivery systems, where the release mechanism is not strictly Fickian diffusion. For our analysis, melittin release was plotted against time raised to an empirical exponent, n, which was chosen as 0.45 as a starting point. The exact value of n can shed light on the drug release mechanism. The error bars, as in the previous models, represent the standard deviation of the melittin measurements.

Cell grouping

All cells were divided into 7 different groups based on the different treatments: Control Group (CG), SKOV3 cells were not treated with nanoparticles or alginate lyase. This group serves as the baseline to compare the effects of treatments in other groups; Alginate Nanoparticles Group (NG), SKOV3 cells were treated with alginate nanoparticles. This group allows us to evaluate the effects of the nanoparticle carrier itself on the cells; melittin Peptide Group (PG), SKOV3 cells were treated with free melittin (not encapsulated in nanoparticles). This group allows us to compare the effects of free melittin vs encapsulated melittin; melittin-encapsulated nanoparticles group (PNG), SKOV3 cells were treated with melittin-encapsulated alginate nanoparticles. This group allows us to assess the effects of melittin encapsulation; melittin-encapsulated Nanoparticles + Lyase Group (PNLG/PNMG/PNHG, 0.1/0.5/1 μM), SKOV3 cells treated with

melittin-encapsulated alginate nanoparticles in the presence of low, middle and high concentrations of alginate lyase. The cell concentrations were determined via cytometer counting after 24 h culture.

Cell viability assay

Cell viability was assessed using the MTT (3-(4,5-dimethylthiazol-2-yl)-2,5-diphenyltetrazolium bromide) method after 1, 2 and 3 d of culture. The cells in the exponential phase were plated in 96-well plates with a density of 10^4 cells/well and treated with SiO_2–alginate–melittin (with 0, 0.1, 0.5, 1, 10 and 100 μM of melittin), or equal volume of SiO_2–alginate solution for 24 h. At the end of culture, 50 μL of MTT (10 mg/mL) was added to each well and for further 4 h incubation. Formazan was dissolved in dimethyl sulfoxide (DMSO), and the absorbing values were measured at 540 nm using a microplate reader (Ortenberg, Germany). The cells were only treated with 0.1% of DMSO as controls. Inhibitory rates were measured using OD values from treated samples divided by those of the controls in percentages.

Measurement of membrane integrity

To assess cell membrane integrity via lactate dehydrogenase (LDH) leakage, cells were seeded at a concentration of 1×10^5 cells/mL in a 96-well plate with 100 μL of culture medium per well and incubated at 37 °C in a 5% CO_2 atmosphere until reaching 70–80% confluency (typically 24 h). Post-confluency, the cells were treated with nanoparticles and incubated for an additional 24 h at 37 °C. Following this incubation, the culture medium was gently aspirated from each well and transferred to 1.5 mL microcentrifuge tubes. This medium was then centrifuged at $400 \times g$ for 5 min at 4 °C to sediment any cellular debris. The clear supernatant was collected, ensuring the pellet was undisturbed. Using an LDH cytotoxicity assay kit, the reaction mixture was prepared as per the manufacturer's guidelines. The supernatant (usually between 50 and 100 μL) was added to a fresh 96-well plate, followed by the addition of the reaction mixture. The plate was incubated for 30 min at room temperature, shielded from light. Absorbance was subsequently measured using a microplate reader at around 490 nm, as typically recommended by LDH assay kits. A spike in LDH activity in the supernatant, relative to controls, indicates potential membrane damage, suggesting possible cytotoxic effects of the nanoparticles on the cells.

Mitochondrial membrane potential analysis

All cell groups should be treated for a consistent duration, ideally 24 h, to standardize the effect of treatments. For the staining process, use JC-1 dye at a concentration of 10 μg/mL (Sivandzade et al 2019). Post-treatment, incubate cells with JC-1 for exactly 20 min at 37 °C in a CO2 incubator to ensure uniform staining. As a control for the staining process, include a subset of cells treated with a known mitochondrial depolarizer carbonyl cyanide m-chlorophenyl hydrazone (CCCP) (Sopha et al. 2023), at a concentration of 50 μM for 30 min. This will act as a positive control for mitochondrial depolarization. Before flow cytometry, wash the cells twice with cold PBS to remove excess dye, maintaining a temperature of 4 °C to prevent any further metabolic changes. For flow

cytometry, use a 488 nm laser for excitation and measure the emission at 530 nm (green) and 590 nm (red).

Flow cytometric analysis for cell uptake

Initially, we prepared Cy3-labeled nanoparticles, ensuring that the labeling efficiency was uniform across batches (Ouyang et al. 2020). The fluorescence intensity of Cy3 was consistently measured and found stable under conditions mimicking the cellular environment. We then proceeded to incubate the SKOV3 cells with these nanoparticles. We chose a concentration of 100 μg/mL for the nanoparticles and incubated the cells for exactly 4 h. This process was conducted at 37 °C in a 5% CO2 incubator, replicating the physiological conditions of the cells. Post-incubation, we performed a triple-wash protocol using cold PBS, keeping the temperature at a constant 4 °C. This temperature was critical to halt any further cellular processes and ensured the removal of non-internalized nanoparticles. Subsequently, the cells were carefully resuspended in PBS at the same temperature. We paid special attention to preserve cell viability and prevent cell aggregation, which could have adversely affected the flow cytometric analysis. We calibrated our flow cytometer to specifically detect the Cy3 fluorescence wavelength, adjusting settings to accurately differentiate Cy3 fluorescence from cellular autofluorescence. Each sample was analyzed for a minimum of 20,000 cells, ensuring a statistically significant sample size for our quantitative analysis. In our analysis, we not only recorded the percentage of cells exhibiting Cy3 fluorescence but also quantified the mean fluorescence intensity, which provided a comprehensive understanding of the nanoparticle uptake. We included a negative control group consisting of cells not exposed to nanoparticles. This control was essential for determining the baseline level of background fluorescence.

Measurement of mitochondrial oxygen consumption rate (OCR)

The Seahorse XF Analyzer was calibrated according to the manufacturer's instructions (Ouyang et al. 2020). SKOV3 cells, post-treatment, were seeded in a Seahorse cell culture microplate at a density of 20,000 cells per well. OCR measurements were taken at 0, 30, 60, 90, and 120 min after introducing the cells to the analyzer. This time series allowed for the assessment of immediate and short-term responses in mitochondrial respiration to the different treatments. During the OCR measurement, the temperature was maintained at 37 °C, and CO2 was excluded to ensure a stable environment for the cells. This setup was critical for accurate OCR readings, as fluctuations in temperature or CO2 levels can affect cellular respiration. The Seahorse software was used to calculate the OCR for each timepoint. The data were normalized to the cell count obtained from a parallel cytometer analysis to account for any differences in cell density across wells. Statistical analysis was performed to compare the OCR values across different timepoints and treatment groups. The mean and standard deviation of OCR values were calculated for each group at each timepoint.

SKOV3 cells were categorized into seven distinct groups: Control Group (CG), Alginate Nanoparticles Group (NG), Melittin Peptide Group (PG), Melittin-Encapsulated Nanoparticles Group (PNG), and three Melittin-Encapsulated Nanoparticles + Lyase Groups with concentrations of 0.1 μM (PNLG), 0.5 μM (PNMG), and 1 μM (PNHG). Each group was cultured 30 min to ensure uniformity in treatment exposure. After

30 min of culture, the stability of the OCR across all groups was verified. The cells were treated with based on the grouping. At 60 min, all cell growth was stable among all groups, and oligomycin (1 μM) was added to inhibit ATP synthase, enabling the measurement of ATP-linked OCR (Ratajczak et al. 2019). At 80 min, all cell growth was stable among all groups, and FCCP (0.5 μM) was introduced to uncouple the mitochondrial respiratory chain, facilitating the assessment of maximal respiration capacity (Sperling et al. 2019). At 100 min, all cell growth was stable among all groups, a combination of Antimycin A (0.5 μM) and Rotenone (0.5 μM) was administered to obstruct the mitochondrial electron transport chain, indicating non-mitochondrial OCR (Pulikkot et al. 2023). All cells were culture 120 min total.

SKOV3 cells were cultured under standardized conditions and seeded in Seahorse XF Analyzer plates at a consistent density of 5×10^4 cells per well to ensure uniformity across measurements. OCR measurements were taken at baseline (0 min) and following the addition of each modulator at each 10 min. This allowed for the tracking of dynamic OCR changes in response to each treatment. OCR readings were normalized to the cell count in each well to account for variations in cell density. The Seahorse software was employed to calculate essential respiratory parameters, including basal respiration, ATP-linked respiration, maximal respiration, and non-mitochondrial respiration for each group.

Assay of ovarian cancer cell migration and invasion

Ovarian cancer cell migration was evaluated using wound-healing assays. The straight artificial scratches were made using 10 μL sterile tips. When the cells grew to 70–80% confluency, the cells spreading across the scratches were measured and taken a photo under a microscope at consecutive at 0, 6, 24 and 36 h timepoint. Relative distance of wounding site was calculated according to the distance at specific timepoints divided by the scratching distance at 0 h in the same group. Transwell coated with Matrigel was used to evaluate ovarian cancer cell SKOV3 invasion. Ovarian cancer cells SKOV3 were resuspended in 100 μL serum-free medium and allowed to invade toward complete cell growth medium for 2 days. The cells attached to the lower membrane surface were fixed using 4% of paraformaldehyde for half an hour, rinsed with PBS solution for two times, and stained with 0.1% of crystal violet for half an hour. The cells were rinsed twice, and the surface of the upper chamber gently dried with a sterile cotton. The invading cells were observed, imaged and counted under a microscope.

ROS detection

ROS Assay Kit was purchased from Beyotime Biotechnology Company, Beijing, China. The first step to an effective ROS detection procedure entailed the preparation of DCFH-DA dilution. The task began with the combination of DCFH-DA and a serum-free culture medium in a ratio of 1:1000. This precise proportion ensures that the final concentration is maintained at an optimal level of 10 μmol/l. Once the DCFH-DA dilution was adequately prepared, the focus shifted to the cell culture. First, we fully drained off the existing cell culture medium. Following this, added the prepared diluted DCFH-DA in a manner that it fully covers the cell layer. Upon successful incorporation of the diluted DCFH-DA into the cell culture, incubation followed. This step entailed placing

the cells in an incubator maintained at a temperature of 37 °C. The incubation period lasted for 20 min, a time frame optimal for ensuring thorough interaction between the cells and the DCFH-DA solution. Post-incubation, it is time to wash the cells meticulously. This required the use of a serum-free cell culture medium. The cells needed to be washed a total of three times to ensure that any residual DCFH-DA solution was completely removed. The final step in this procedure involved direct observation of the cells under an inverted fluorescent microscope. Make sure to capture images of the cells for record-keeping and further analysis.

Apoptosis marker measurement

Apoptosis was determined by measuring the expression of apoptosis-related proteins (Bcl-2, Bax, Caspase-3) using qPCR and Western blotting. For qPCR analysis, RNA was extracted using an RNA extraction kit, following the manufacturer's instructions, typically involving cell lysis, phase separation, washing, and elution. The RNA was then reverse transcribed into cDNA at 42 °C for 1 h using a reverse transcription kit. qPCR was set up with specific primers for Bcl-2, Bax, Caspase-3, and a housekeeping gene, such as GAPDH, following the manufacturer's recommendations. The cycling conditions included an initial denaturation at 95 °C for 3 min, followed by 40 cycles of denaturation at 95 °C for 15 s and annealing/extension at 60 °C for 1 min. Data were analyzed using the $^{\Delta\Delta}$Ct method, normalized to the housekeeping gene, and relative expression levels were calculated. Apoptosis markers were determined by first extracting proteins from cells using RIPA buffer (1 mL per 10^7 cells) with protease and phosphatase inhibitors, incubated on ice for 30 min. The lysate was then centrifuged at 14,000 × g for 15 min at 4 °C to collect the protein supernatant. Protein separation was performed using 10 or 12% SDS–PAGE (30–50 μg per well) at 120 V for 90 min, followed by transfer to a PVDF membrane at 100 V for 60 min. The membrane was blocked with 5% non-fat milk for 1 h and incubated with primary and secondary antibodies as previously described. Visualization was achieved using an enhanced chemiluminescence system for 1–5 min.

Statistical analysis

SPSS 20.0 (IBM, USA) was used for data analysis. All data were expressed as mean ± standard deviation (S.D.), and two groups were compared using a t test. $P < 0.05$ was considered statistically significant.

Results and discussion

Characterization of melittin and SAMNs

SAMNs and SiO_2 nanoparticles were observed using SEM, respectively. The morphology of both SAMNs and SiO_2 nanoparticles, as observed under microscopy, predominantly features a spherical structure with diameters 209.0 ± 48.9 nm. SEM shows the smooth surface of SiO_2 nanoparticles and rough surface of SAMNs with more aggregation (Fig. 1A). The density plot for SAMN nanoparticles demonstrates a broader size distribution, indicating a greater variability in particle sizes. In contrast, the SiO_2 nanoparticles exhibit a narrower size distribution, with a higher density around smaller size ranges (Fig. 1B). This suggests a more uniform particle size, which is typical for single-component nanoparticles, such as SiO_2. HPLC analysis indicates that the purity of synthesized

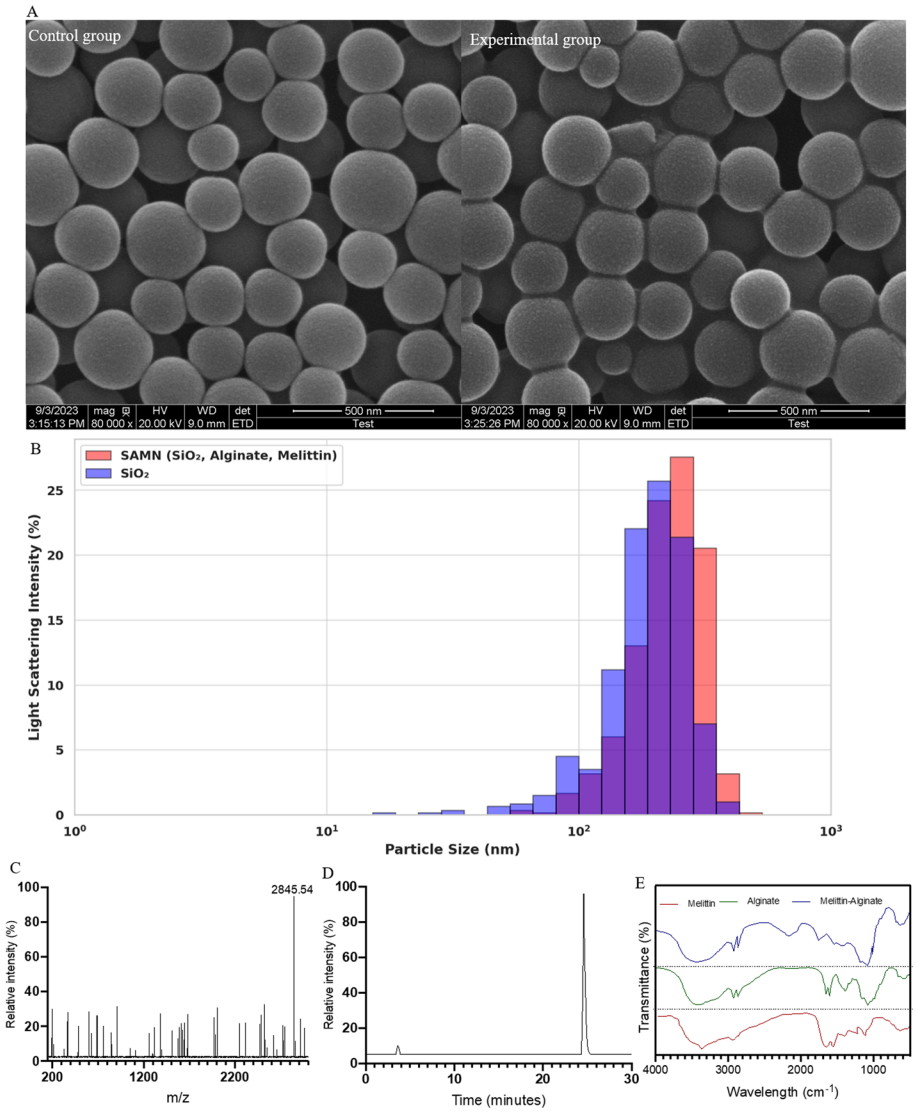

Fig. 1 Characterization of melittin, alginate and melittin–alginate conjugation. **A**, scanning electron microscopy (SEM) analysis of the morphology of SiO_2 nanoparticles (left) and SiO_2–alginate–melittin nano-conjugates (right). **B**, Red bars represent the size distribution and light scattering intensity of SAMN nanoparticles. The blue bars illustrate the size distribution and light scattering intensity of SiO_2 nanoparticles. **C**, HPLC analysis of synthesized melittin. **D**, ESI–MS analysis of synthesized melittin. **E**, FTIR spectra of synthesized molecules of melittin, alginate and melittin–alginate conjugation

melittin is more than 95% and other peptides contaminated (Fig. 1C). ESI–MS spectrum shows that the molecular weight of melittin is 2846, since the mass is measured in a negative ion mode, which is accordant with its theoretical molecular weight (Fig. 1D). For melittin, there is an obvious absorbing region of 3400–3500 cm^{-1}, indicating the free vibrations of an NH group. There are the absorbing peaks with the vibration's amide I (1650 cm^{-1}), amide II (1552 cm^{-1}), and coil conformation (1220 cm^{-1} and 1114 cm^{-1}) (Fig. 1E). For alginate, there are the overlapped OH (3435 cm^{-1}), CH group (2925 and 2870 cm^{-1}), and CO group (1088 cm^{-1}) (Zheng et al. 2011). In the FT-IR spectrum of melittin–alginate conjugates, the melittin absorbing peak for a NH group at the region of 3400–3500 cm^{-1} is reduced (Fig. 1E). CH group (2925 and 2870 cm^{-1}) and CO group

(1088 cm^{-1}) can be observed. The amide I vibrations at 1650 cm^{-1} are increased in the conjugates. In the SiO_2 infrared absorption spectrum, the strong absorption (Si-O-Si antisymmetric stretching vibration) was existed at 1091 cm^{-1}, and Si-O bond symmetric stretching vibration was existed at 797 cm^{-1}. The changes in the infrared absorption spectra of the functional groups of SiO_2, alginate, melittin and SiO_2/alginate/melittin further proved that alginate and melittin were successfully loaded into SiO_2 nano-conjugates (Fig. 1E). Through electron microscopy characterization and XRD component analysis, the characteristics of the SAMN were confirmed.

Cytotoxic effects of melittin, SAMNs, and alginate lyase on SKOV3 Cells

Melittin demonstrates a dose-responsive cytotoxic influence on SKOV3 cancer cells. At nominal concentrations (0.1 μM), the metabolic activity of these cells remains analogous to the control, signifying negligible cytotoxicity. However, with escalating melittin concentrations, particularly at 1 μM and beyond, there is a marked reduction in cell viability, underscoring its intensified cytotoxic implications. At elevated concentrations, specifically 10 and 100 μM, cell viability is nearly obliterated, emphasizing melittin's potent cytotoxicity on SKOV3 cells at these dosages (refer to Fig. 2A). Subsequent to a 24 h culture period, the impacts of SAMNs and alginate lyase on SKOV3 cells were assessed. Observations revealed that cell concentrations across CG, NG, PNG, PNLG, and PNMG groups remained statistically consistent post the 24 h culture. However,

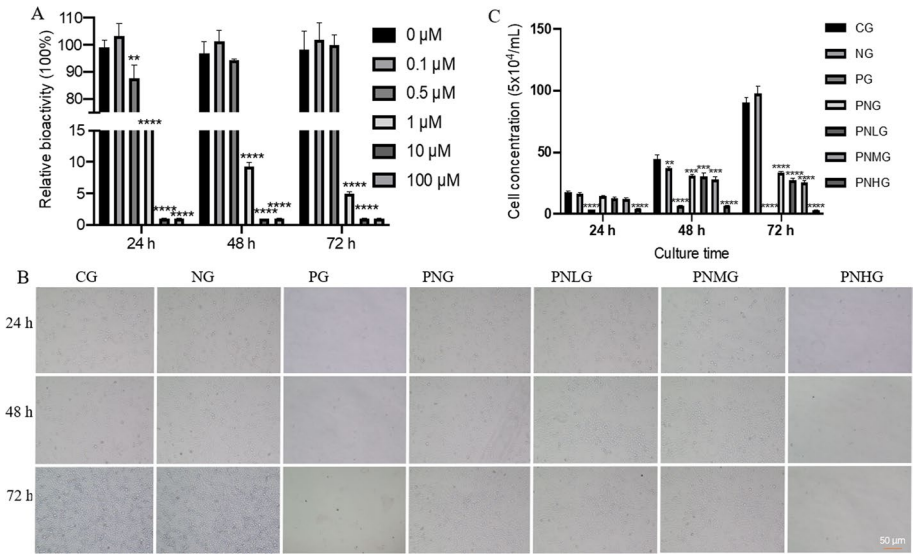

Fig. 2 Cytotoxic effects of melittin, SAMNs, and alginate lyase on skov3 cells over different culture periods. **A**, dose-responsive cytotoxicity of melittin on SKOV3 cells. **B**, comparative cell concentrations post a 24 h culture across different groups. **C**, a detailed representation of cell concentrations in different groups. The cells were divided into seven groups: Control Group (CG), SKOV3 cells were not treated with nanoparticles or alginate lyase; Alginate Nanoparticles Group (NG), SKOV3 cells were treated with alginate nanoparticles; melittin Peptide Group (PG), SKOV3 cells were treated with free melittin (not encapsulated in nanoparticles); melittin-Encapsulated Nanoparticles Group (PNG), SKOV3 cells were treated with melittin-encapsulated alginate nanoparticles; and melittin-Encapsulated Nanoparticles + Lyase Groups (PNLG/PNMG/PNHG, 0.1/0.5/1 μM lyase), SKOV3 cells treated with melittin-encapsulated alginate nanoparticles in the presence of low, middle and high concentrations of alginate lyase. $n = 3$ for each group. $^{**}P < 0.05$, $^{***}P < 0.05$, and $^{****}P < 0.05$ vs the CG group

notably diminished concentrations were evident in the PG and PNLG clusters (see Fig. 2B, C, $P < 0.0001$). Cellular disruption and digestion were predominant in these two groups (Fig. 2B). Post the 48 and 72 h intervals, remnants of disrupted cells were discernible solely in the PG and PNHG groups. Conversely, the CG and NG groups exhibited consistent cell concentrations post the 24- and 72-h culture periods. This indicates that nanoparticles alone do not induce cytotoxicity. Maximum cellular toxicity was observed when 1 μM alginate lyase was employed in PNHG, mirroring the effects observed when 1 μM melittin was utilized in the PG group.

Mitochondrial membrane potential

In the analysis of mitochondrial membrane potential via the JC-1 dye assay, the results from Fig. 3A, B indicate distinct responses among the SKOV3 cell treatment groups. The CG group maintained a high mitochondrial membrane potential with red to green fluorescence ratios averaging around 20, suggesting healthy and intact mitochondrial function. The NG group also showed high ratios, similar to the CG, indicating that the alginate nanoparticle treatment alone did not significantly affect the mitochondrial membrane potential of the cells. Contrastingly, the PG group exhibited a stark decrease in the red to green fluorescence ratio, averaging around 0.01, which signifies a severe disruption of mitochondrial membrane integrity due to the treatment with free melittin. This is consistent with the known cytotoxic effects of melittin, which can disrupt mitochondrial integrity and function (Harfmann and Florea 2023). The PNG group displayed intermediate ratios, with an average close to 1, indicating a partial reduction in mitochondrial membrane potential, thus suggesting that encapsulation of melittin reduces its cytotoxic impact. Furthermore, the addition of alginate lyase in the (PNLG, PNMG, and PNHG) revealed a dose-dependent decrease in the mitochondrial membrane potential, with the lowest ratio observed in the PNHG, where the highest concentration of lyase was applied. This dose-dependent trend underscores the potential interaction between alginate lyase and alginate nanoparticle, and the encapsulated melittin, affecting the compound's impact on mitochondrial stability. The results are also consistent with the previous reports the degradation of the alginate microfibers was controllable and tunable with alginate lyase (Keaswejjareansuk et al. 2021).

Cell uptake of nanoparticles

The fold change values for cell uptake of nanoparticles obtained from the Seahorse XF Analyzer (Fig. 3C, D). The CG group, with no treatment applied, had the highest cell uptake values, with fold changes exceeding 32, indicating the baseline uptake rate of healthy cells. Similarly, the NG group displayed high cell uptake values, with fold changes ranging from 29.01 to 33.59, suggesting that the presence of alginate nanoparticles did not drastically impair mitochondrial cell uptake functions. In contrast, the PG group showed the lowest cell uptake fold changes, with values around 1.19 to 1.3, indicating a substantial decrease in the function. This suggests that free melittin significantly inhibits cellular function. However, as melittin is encapsulated in nanoparticles (PNG), the cell uptake fold change increases, averaging around 22, which points to a mitigated effect of melittin on respiration due to the encapsulation process. The previous work also showed that nanoparticle can change cancer

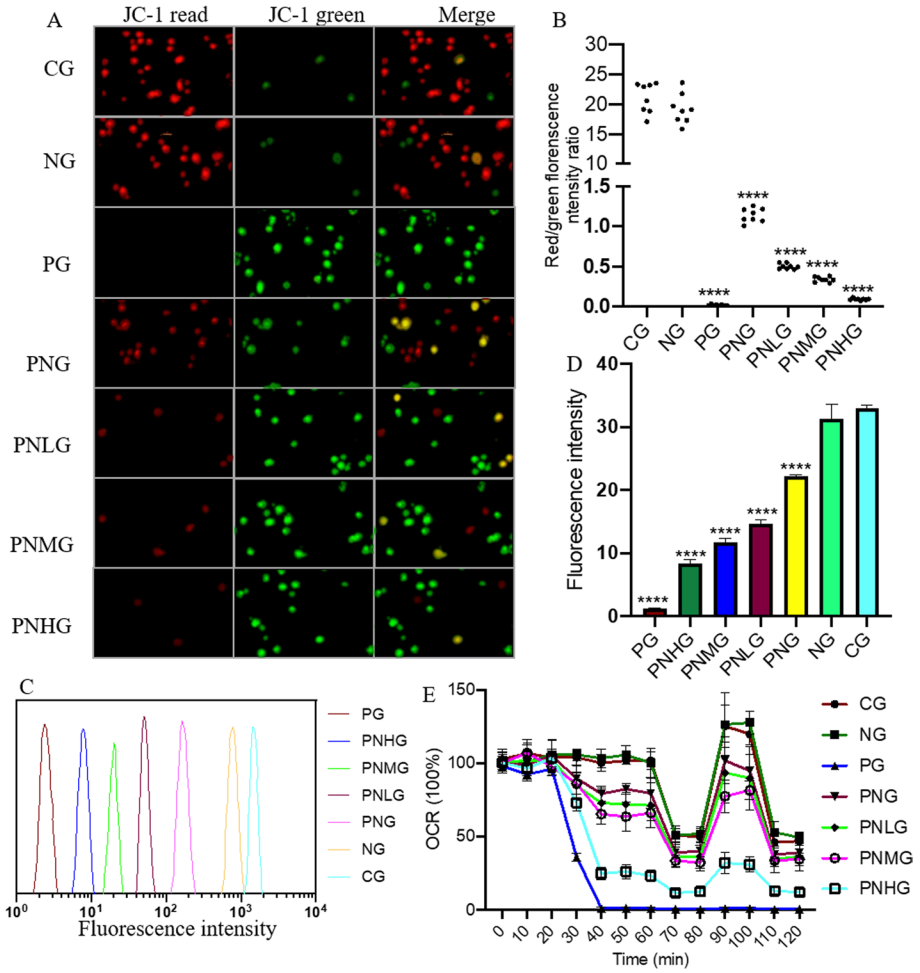

Fig. 3 Impact of nanoparticles on mitochondrial functions in SKOV3 cells. This figure presents a comprehensive analysis of how various nanoparticle treatments influence mitochondrial dynamics within SKOV3 ovarian cancer cells. Panels **A** and **B** detail the mitochondrial membrane potential, utilizing JC-1 staining to provide a comparative visualization of membrane polarization across different treatment groups. **A** higher red to green fluorescence ratio indicates a more polarized, and thus healthier, mitochondrial state. Panels **C** and **D** offer insights into the cellular uptake of nanoparticles, essential for understanding the intracellular delivery efficiency and subsequent bioactivity of the nanoparticles. Panel E presents the results of a comprehensive study measuring the OCR of SKOV3 cells subjected to various treatments using a Seahorse XF Analyzer. The cells were divided into seven groups: Control Group (CG), Alginate Nanoparticles Group (NG), Melittin Peptide Group (PG), Melittin-Encapsulated Nanoparticles Group (PNG), and Melittin-Encapsulated Nanoparticles + Lyase Groups at concentrations of 0.1 μM (PNLG), 0.5 μM (PNMG), and 1 μM (PNHG). Measurements were taken at intervals of 10 min over a period of 120 min, encompassing baseline readings and subsequent response to the addition of mitochondrial respiration modulators: nanoparticle treatment at 30 min, Oligomycin (inhibitor of ATP synthase) at 60 min, FCCP (uncoupler of mitochondrial respiration) at 80 min, and a combination of Antimycin A and Rotenone (inhibitors of the electron transport chain) at 100 min. The data illustrate the dynamic changes in mitochondrial respiration across different treatment groups, highlighting the significant impact of melittin, both in free and encapsulated forms, on mitochondrial function compared to the control and alginate nanoparticle-treated groups

cell uptake (Bai et al. 2020; Hui et al. 2020). Moreover, the presence of alginate lyase in combination with melittin-encapsulated nanoparticles (PNLG, PNMG, and PNHG) showed a dose-dependent increase in cell uptake fold change. The highest cell uptake values were noted in the PNLG group, with a peak value of 15.11, while

the PNMG and PNHG groups exhibited moderately high cell uptake fold changes of around 11–12 and 7–9, respectively. These results suggest that alginate lyase, when combined with encapsulated melittin, has a complex effect on cellular uptake, which may be related to the concentration of lyase used and its potential impact on the release of melittin from the nanoparticles.

Mitochondrial respiration in SKOV3 cells

Baseline and Early Timepoints (0–20 min), initially, all groups, including the Control Group (CG), Alginate Nanoparticles Group (NG), Melittin Peptide Group (PG), Melittin-Encapsulated Nanoparticles Group (PNG), and Melittin-Encapsulated Nanoparticles + Lyase Groups at varying concentrations (PNLG, PNMG, PNHG), exhibited similar OCR values. This indicates a uniform mitochondrial respiration rate across all groups before the application of specific modulators. The slight fluctuations in OCR values between 10 and 20 min across different groups suggest minor variations in basal mitochondrial activity, which is typical in cellular assays (Fig. 3E).

Post-nanoparticle Treatment (30–50 min), a significant decline in OCR was observed in the PG group after 30 min, indicating a drastic reduction in mitochondrial respiration due to the effect of melittin. This effect was even more pronounced at the 40- and 50-min marks, with near-zero OCR values, signifying a complete loss of mitochondrial function. Contrastingly, the CG and NG groups maintained relatively stable OCR levels, suggesting that alginate nanoparticles alone do not significantly affect mitochondrial respiration (Fig. 3E). Post-Oligomycin Treatment (60–70 min), the introduction of oligomycin, an ATP synthase inhibitor, resulted in a marked decrease in OCR across all groups, reflecting the expected inhibition of ATP-linked respiration. The PG group maintained negligible OCR levels, consistent with previous observations of melittin's impact on mitochondrial function (Fig. 3E). FCCP Treatment (80–90 min), the addition of FCCP, a mitochondrial uncoupler (Khailova et al. 2020), should typically lead to an increase in OCR as it stimulates maximal respiration. However, only the CG, NG, and PNG groups showed this expected increase, with the CG group reaching the highest levels, indicating robust mitochondrial function. The persistent low OCR in the PG group underscores the profound inhibitory effect of melittin on mitochondrial respiration (Fig. 3E). Post-Antimycin A and Rotenone Treatment (100–120 min), following the addition of Antimycin A and Rotenone, which block the mitochondrial electron transport chain (Cheng et al. 2020; Mazibuko-Mbeje et al. 2021), a decrease in OCR was observed across all groups. This is indicative of the inhibition of non-mitochondrial respiration. The continuous minimal OCR in the PG group reiterates the significant impact of melittin on mitochondrial functionality. In conclusion, these results demonstrate the variable effects of different treatments on mitochondrial respiration in SKOV3 cells. Melittin, particularly in its free form, exhibited a profound inhibitory effect on mitochondrial function, whereas alginate nanoparticles and their melittin-encapsulated forms showed comparatively moderate impacts. These findings provide crucial insights into the mitochondrial dynamics of SKOV3 cells under various experimental conditions.

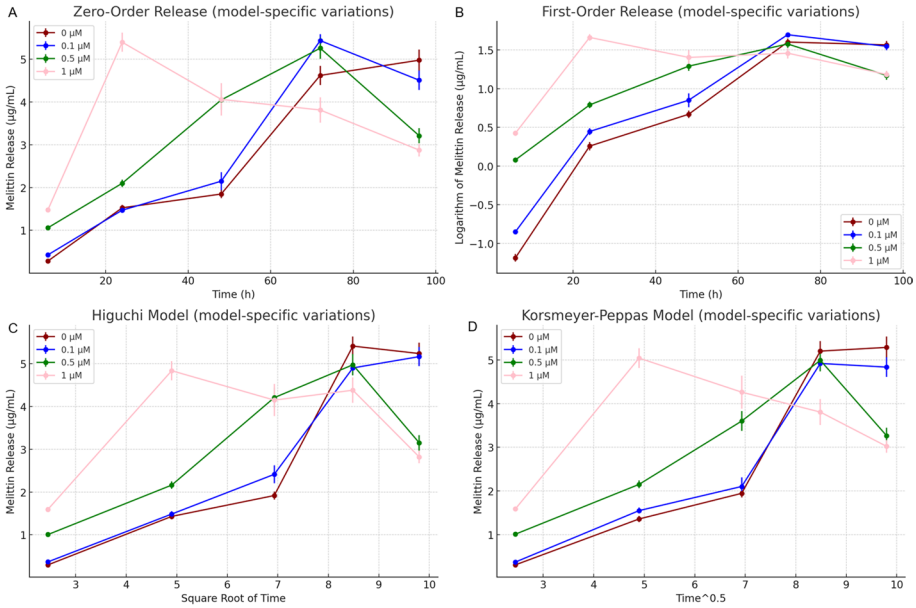

Fig. 4 Release kinetics of melittin in the presence of varying concentrations of alginate lyase. **A**, Zero-Order Release of melittin over time. The error bars represent the standard deviation of three measurements. **B**, First-Order Release represented by the natural logarithm of melittin concentration against time. **C**, Release profile based on the Higuchi Model, plotting melittin release against the square root of time. **D**, Korsmeyer–Peppas Model showing melittin release against time raised to the power of 0.45. $n = 3$ for each group

Release kinetics of melittin

In zero-order release, the melittin release is shown against time for various alginate lyase concentrations (Fig. 4A). A true zero-order release would be represented by a straight line, indicating a constant release rate. For the 0 μM concentration of alginate lyase, we observe an initial increase followed by a plateau and then a decrease, suggesting a possible saturation or degradation effect. The concentrations with alginate lyase show varying release profiles, with the 1 μM concentration demonstrating a more rapid release initially, which could be attributed to the enzyme's enhanced activity at this concentration. However, none of the profiles seem to adhere strictly to a zero-order kinetic model throughout the entire time frame. The natural logarithm of melittin release is plotted against time. A linear relationship would indicate first-order kinetics, where the release rate is proportional to the remaining melittin concentration. While there is some linearity in the initial stages, especially for the 0.5 and 1 μM alginate lyase concentrations, none of the profiles consistently align with a straight line over the entire duration, suggesting that the release does not strictly follow first-order kinetics throughout (Fig. 4B). Here, melittin release is plotted against the square root of time. This model describes drug release from insoluble matrices as a diffusion-driven process. While the profiles for alginate lyase concentrations, especially 0.5 and 1 μM, show some linear characteristics in the initial phases, they deviate later on. This suggests that while diffusion might play a role in the initial release stages, other mechanisms or factors influence the release at later timepoints (Fig. 4C). It is pertinent to note that melittin is embedded within alginate polymers, which undergo degradation by alginate lyase. This enzymatic action plays a crucial role in the release dynamics. As the concentration of alginate lyase increases,

there is a more pronounced breakdown of the polymers, leading to a higher initial release of melittin from the nanoparticles. This initial phase of rapid release subsequently tapers off, resulting in a reduced rate of melittin release at later stages. This observation aligns with our findings illustrated in Fig. 4C, where melittin release is modeled as a function of time, demonstrating a distinct release pattern influenced by the enzymatic degradation of alginate polymers. Melittin release is plotted against time raised to an empirical power, in this case, 0.45. This model can help decipher the mechanism of drug release, especially from polymeric systems. A straight line in such a plot might indicate a combination of diffusion and erosion mechanisms. The profiles, particularly for the 0.5 and 1 μM alginate lyase concentrations, show some linearity in the initial stages but deviate later, suggesting a complex release mechanism that might involve both diffusion and other processes (Fig. 4D). Although none of the models perfectly describe the melittin release kinetics over the entire duration, they provide valuable insights (Fig. 4). The presence of alginate lyase, especially at higher concentrations, appears to accelerate melittin release initially. However, the later stages of release are influenced by factors beyond just the enzyme concentration, possibly including nanoparticle degradation, saturation effects, or melittin interactions with the surrounding medium. Further studies might be required to elucidate these mechanisms fully.

LDH release profiles indicative of cell membrane integrity

The LDH release plots for individual concentrations of alginate lyase over time provide insights into the potential impact on cell membrane integrity (Sreenivasan et al 2021). At 0 μM, LDH levels exhibit fluctuations (Fig. 5A), suggesting no clear correlation with time. The 0.1 μM concentration depicts a relatively stable LDH release, indicating minor to no significant disruptions to the cell membrane (Fig. 5B). However, at 0.5 μM, there is an evident peak and subsequent decrease, hinting at a transient effect on the cell membrane (Fig. 5C). The 1 μM concentration showcases an initial spike in LDH release (Fig. 5D), which stabilizes after 48 h, implying a possible adaptive cellular response. The comprehensive graph amalgamates the LDH release profiles across all alginate lyase concentrations. It serves as a comparative tool, emphasizing that the 1 μM concentration might have the most substantial impact on membrane integrity (Fig. 5E). This conclusion is drawn from the notable initial rise in LDH release at this concentration. Boxplots shed light on the distribution and variability of the LDH release data. At 0 μM, there is a discernible variability in LDH measurements, especially around the 72 h mark (Fig. 5F). The 0.1 μM concentration mostly exhibits a compact distribution, barring the 48 h timepoint (Fig. 5G). The 0.5 μM data set shows variability, particularly at 48 and 96 h (Fig. 5H). Finally, the 1 μM concentration demonstrates consistency with noticeable outliers at specific timepoints, suggesting occasional spikes in membrane disruptions (Fig. 5I).

The LDH release, an indicator of cell membrane damage, varies across the different concentrations of alginate lyase. The increase in LDH release at higher concentrations, particularly at 1 μM, suggests potential membrane damage (Fig. 5). However, it is essential to note that the LDH levels appear to stabilize after a certain period, indicating that the cells might either adapt or reach a saturation point in response to the nanoparticles. The variability in measurements, as seen in the shaded regions and boxplots, emphasizes

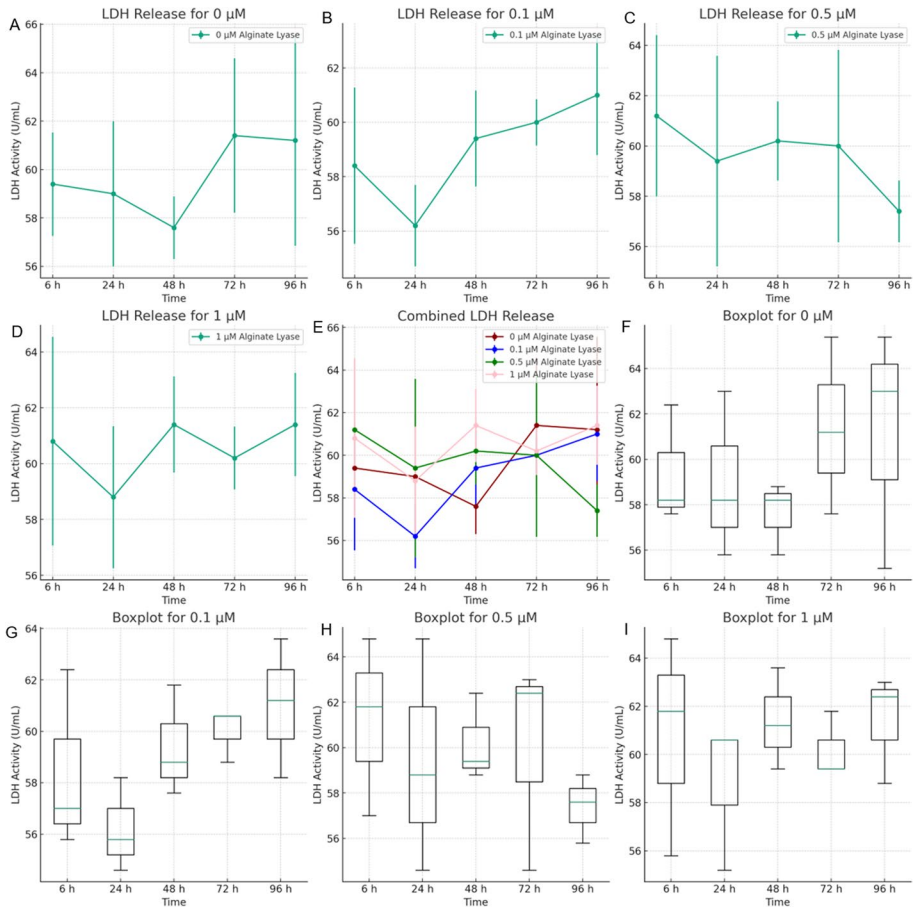

Fig. 5 LDH release profiles indicative of cell membrane integrity across different concentrations of alginate lyase. **A**–**D**, individual LDH release profiles over time for different alginate lyase concentrations, respectively. The shaded regions represent variability between the three measurements for each timepoint. **E**, combined LDH release profile showcasing comparative trends across all alginate lyase concentrations over time. **F**–**I**, boxplots illustrating the distribution of LDH release for each timepoint at different alginate lyase concentrations, respectively. The box represents the interquartile range, the line inside the box denotes the median, and whiskers extend to the most extreme data points not considered outliers. $n = 3$ for each group

the importance of conducting multiple replicates to ensure the accuracy of the findings. In summary, while there is evidence of potential membrane damage, especially at higher concentrations, the cells' adaptive responses or saturation effects might limit the extent of damage over prolonged exposure.

Alginate lyase treatment inhibited cancer cell migration and invasion only treated with SAMN

The effects of SAMN and melittin on SKOV3 cancer cell migration and invasion were assessed through wound-healing and invasion assays. Results revealed that treatment with melittin and high-level alginate lyase-treated SAMN significantly increased the relative distance of wounding sites in the PG and PNHG groups compared to other groups after 6-, 24-, and 36-h culture periods (Fig. 6A, B, $P < 0.0001$). This distance exhibited a positive correlation with the concentration of alginate lyase. Especially, melittin alone increased the wounding distance and showed the highest cytotoxicity, posing potential

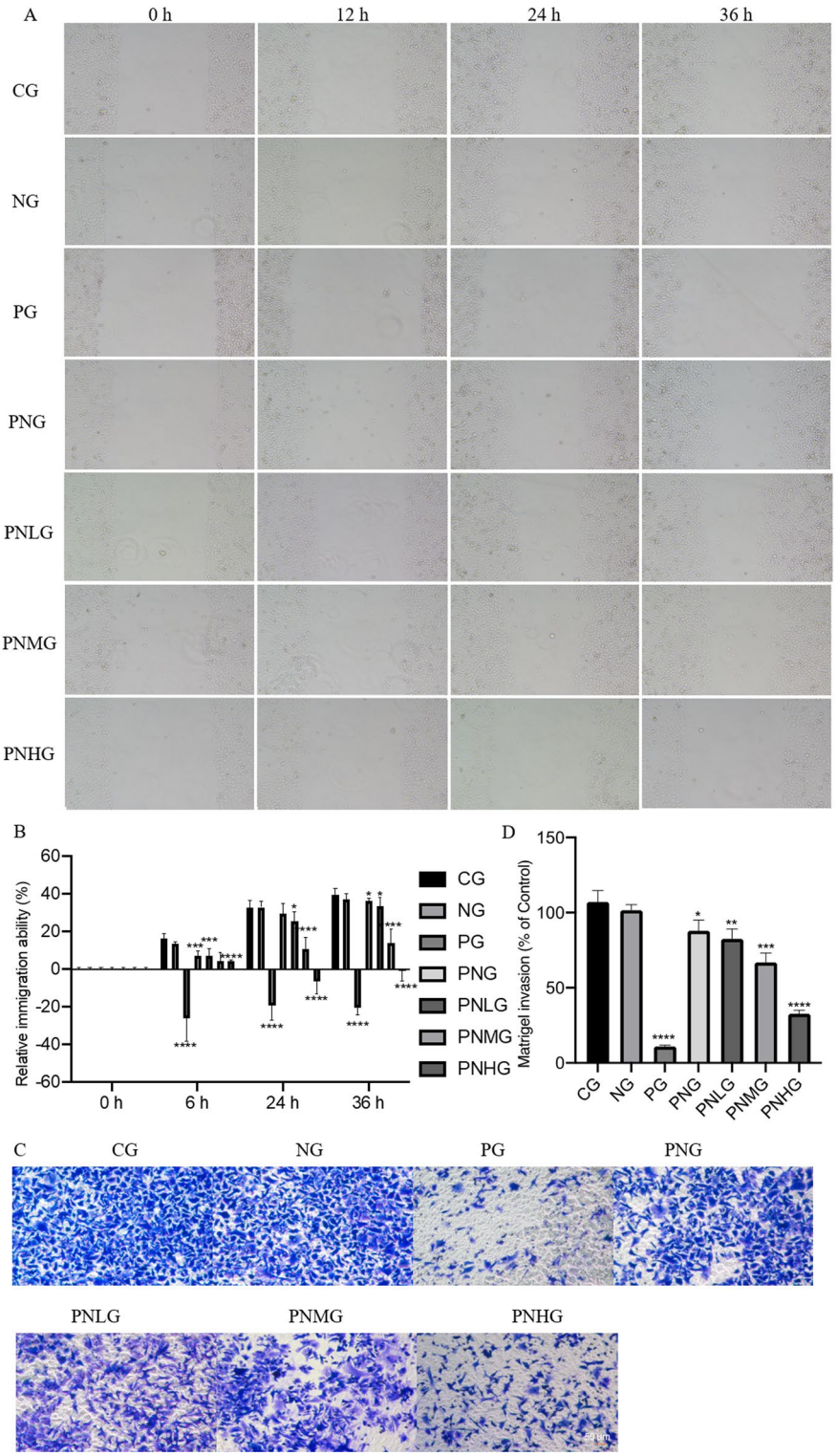

Fig. 6 Effects of melittin, alginate lyase and SiO_2–alginate–melittin conjugation on the cell migration and invasion in the ovarian cells SKOV3. **A**, migration of ovarian cancer cells among different groups after 0-, 6-, 24- and 36 h culture. **B**, relative distance of wound sites among different groups. **C**, cell invasion among different groups. **D**, invading cell numbers among different groups. $n = 3$ for each group. $^{*}P < 0.05$, $^{**}P < 0.01$, $^{***}P < 0.001$, and $^{****}P < 0.0001$ vs the CG group

harm to normal cells. The invasion assay corroborated these findings, with melittin and high-level alginate lyase-treated SAMN resulting in fewer invading cells in the PG and PNHG groups after 24 h culture (Fig. 6C, D, $P < 0.0001$). The number of invading cells negatively correlated with the concentration of alginate lyase. Collectively, these results suggest that alginate lyase treatment, in conjunction with SAMN, inhibits cancer cell migration and invasion in a concentration-dependent manner. The cytotoxic effects of melittin may be modulated by adjusting the concentration of alginate lyase in the SAMN treatment, offering a potential therapeutic avenue.

The study demonstrates that both melittin and high-level alginate lyase-treated SAMN have significant effects on inhibiting cancer cell migration and invasion. The increase in the relative distance of wounding sites and the decrease in the number of invading cells indicate the effectiveness of these treatments. The positive relationship between the distance of wounding sites and the concentration of alginate lyase, along with the negative relationship with the number of invading cells, suggests a concentration-dependent effect. This implies that careful calibration of alginate lyase concentration could optimize the therapeutic effects. While melittin alone increased the distance between wounding sites, it also exhibited the highest cytotoxicity. This raises concerns about its potential harm to normal cells, indicating that melittin's application as a therapeutic agent may require careful consideration and control. The combined treatment of alginate lyase with SAMN appears to be an approach to inhibit cancer cell migration and invasion. The ability to control melittin's effects by adjusting the concentration of alginate lyase adds flexibility and precision to this therapeutic strategy.

Alginate lyase addition increased ROS levels in SKOV3 Cells treated by SAMN

In an experiment involving SKOV3 cells, the impact of alginate lyase on ROS levels was investigated, particularly in conjunction with SAMN treatment. The study revealed that both melittin and SAMN, when combined with high concentrations of alginate lyase, significantly elevated ROS levels in PG and PNHG groups compared to other groups after 1 day of culture (Fig. 7, $P < 0.0001$). A concentration-dependent increase in ROS levels was observed with the escalation in alginate lyase concentration. These findings underscore that SAMN influences ROS levels in SKOV3 cells, and that alginate lyase treatment amplifies these levels by facilitating the release of melittin. Conversely,

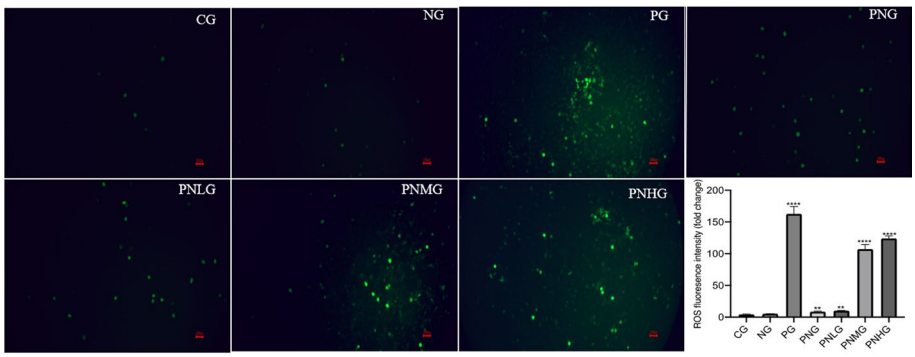

Fig. 7 Effects of melittin, alginate lyase and SiO_2–alginate–melittin conjugation on ROS levels of ROS in cancer cells SKOV3. $n = 3$ for each group. $^{**}P < 0.05$, and $^{****}P < 0.0001$ vs the CG group

the presence of only nanoparticles may restrict melittin's release, thereby limiting the increase in ROS levels. This insight into the role of alginate lyase in modulating ROS levels in SKOV3 cells treated with SAMN offers valuable information for understanding the underlying mechanisms and potential therapeutic applications.

ROS play a complex and multifaceted role in cancer biology (Perillo et al. 2020), acting as a double-edged sword (Wang et al. 2021). On one hand, ROS scavenging can protect healthy cells from oxidative damage and may be leveraged as a preventive strategy against cancer initiation. On the other hand, ROS accumulation can be harnessed for therapeutic purposes, as excessive ROS levels can induce apoptosis in cancer cells (Ansari et al. 2018; Nakamura and Takada 2021). The most stimulating roles of melittin are capable of increasing the oxidative stress by producing ROS, which may be effective against certain cancers (Okon and Zou 2015). melittin, a peptide found in bee venom, has been shown to significantly increase ROS generation, thereby enhancing oxidative stress. This property of melittin may be exploited as an effective anticancer strategy against certain types of cancer, including SKOV3 cells. By promoting ROS production (Fig. 7), melittin can disrupt the redox balance within cancer cells, leading to oxidative damage and cell death. However, the application of melittin in cancer therapy is not without challenges. Alginate nanoparticles, which are often used to encapsulate and deliver melittin, may inadvertently limit its function by preventing its release. This encapsulation can hinder the interaction between melittin and cancer cells, thereby reducing its ability to induce ROS and exert its anticancer effects. The addition of alginate lyase offers a potential solution to this problem. By breaking down the alginate nanoparticles, alginate lyase can facilitate the release of melittin, allowing it to interact with cancer cells and induce ROS production. The concentration of alginate lyase can be carefully adjusted to modulate the release of melittin, providing a means to fine-tune the therapeutic effects.

SAMN with alginate lyase affected the levels of biomarkers of apoptosis in SKOV3 cells

To assess the impact of SAMN combined with alginate lyase on apoptosis biomarkers in SKOV3 cells, the levels of caspase-3, BAX, and Bcl-2 were analyzed. The cells were treated with SAMN and different concentrations of alginate lyase for a 24-h period to specifically evaluate the influence of alginate lyase on the nano-conjugates. The results revealed that only SAMN or high-level alginate lyase treatment increased caspase-3 (Fig. 8A) and BAX relative mRNA levels (Fig. 8B) in the PG and PNHG groups, significantly higher than other groups ($P < 0.0001$). This increase was positively correlated with the concentration of alginate lyase. Conversely, SAMN or high-level alginate lyase treatment reduced Bcl-2 mRNA levels (Fig. 8C) in the PG and PNHG groups, again significantly higher than other groups ($P < 0.0001$), with Bcl-2 levels decreasing as alginate lyase concentration increased. Western Blot analysis (Fig. 8D–G) confirmed these trends. Overall, the findings suggest that SAMN influence apoptosis biomarkers in SKOV3 cells, and alginate lyase treatment enhances apoptosis stress by facilitating the release of melittin in a concentration-dependent manner.

The present study makes a significant contribution to the field of ovarian cancer treatment by SAMNs and evaluating their impact on SKOV3 ovarian cancer cells. Recognizing the potent inhibitory effects of melittin on ovarian cancer and the challenges associated with its instability and potential unintended cell damage, the study

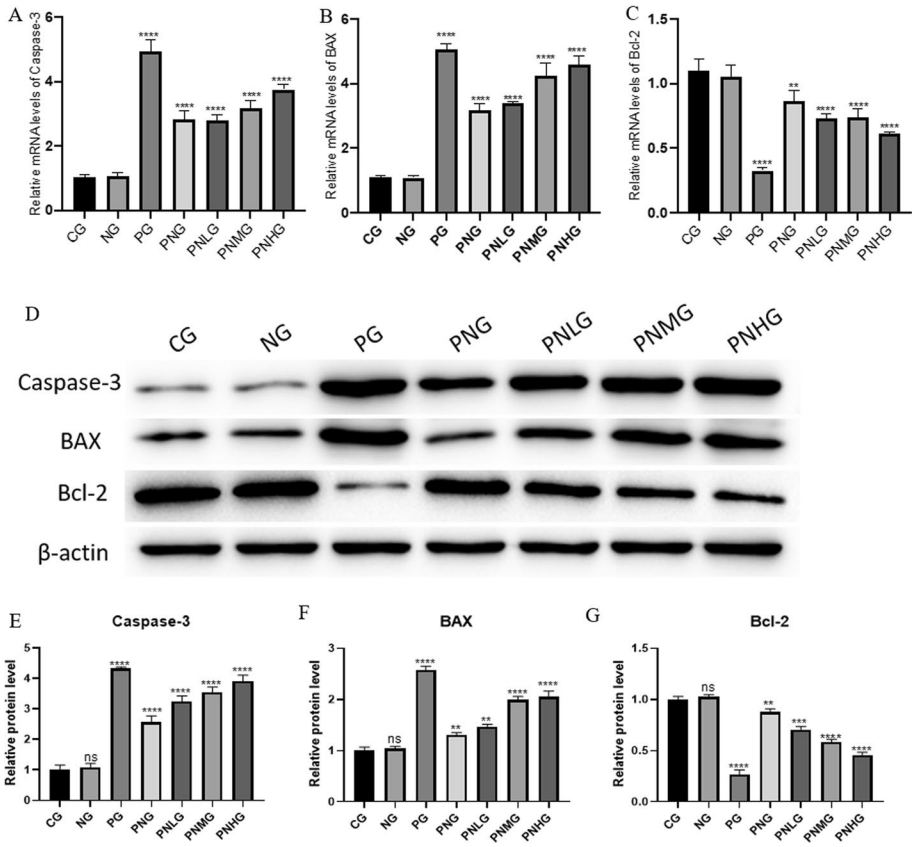

Fig. 8 Effects of melittin, alginate lyase and SiO_2–alginate–melittin conjugation on apoptotic biomarkers levels in cancer cells SKOV3. **A**, relative mRNA level of Caspase-3. **B**, relative mRNA level of MAX. **C**, relative mRNA level of Bcl-2. **D**, Western blot. **E**, relative protein level of Caspase-3. **F**, relative protein level of MAX. C, relative protein level of Bcl-2. $n = 3$ for each group. $^{**}P < 0.01$, $^{***}P < 0.001$, and $^{****}P < 0.0001$ vs the CG group

innovatively integrates melittin and alginate with mesoporous silica. By employing alginate lyase, the researchers facilitated a release of melittin, extending its retention time for cell proliferation control from 1 to 3 days and postponing invasion and migration from 6 to 36 h, compared to melittin alone. The study further demonstrated that SAMNs elevated ROS levels, upregulated Bax and caspase-3 expression, and suppressed Bcl-2 expression, with reduced off-target cytotoxic effects under specific concentrations of alginate lyase. These findings underscore the potential of SAMNs for ovarian cancer cell control, addressing critical challenges in treatment resistance and off-target effects. The incorporation of alginate lyase into the nano-conjugates represents a novel approach that may pave the way for more targeted and effective therapeutic interventions in ovarian cancer.

The study on the impact of SAMN combined with alginate lyase on apoptosis biomarkers in SKOV3 cells reveals a complex interplay between these treatments and the cellular response. By analyzing the levels of caspase-3, BAX, and Bcl-2 following a 24-h treatment with SAMN and varying concentrations of alginate lyase, the study uncovers a nuanced picture of how these components interact. The increase in caspase-3 and BAX relative mRNA levels in the PG and PNHG groups (Fig. 8A, B, $P < 0.0001$) with SAMN or high-level alginate lyase treatment indicates an activation of the intrinsic apoptosis

pathway. This is further supported by the corresponding decrease in Bcl-2 mRNA levels (Fig. 8C), a known anti-apoptotic protein. The positive correlation between the concentration of alginate lyase and the levels of pro-apoptotic markers suggests a dose-dependent effect, which is confirmed by Western Blot analysis (Fig. 8D–G). The underlying mechanism may involve the role of alginate lyase in facilitating the release of melittin, a known cytotoxic agent. By enhancing the release of melittin, alginate lyase may be amplifying the apoptotic stress on the SKOV3 cells. This could explain the observed concentration-dependent effects, where higher levels of alginate lyase lead to increased apoptosis markers. However, the results also raise questions that warrant further investigation. For instance, the specific interaction between SAMN and alginate lyase, and how this combination affects the release and activity of melittin, remains to be elucidated. Understanding the precise molecular targets and signaling pathways involved could provide valuable insights into the therapeutic potential of this approach.

Study limitations

The study focusing on SAMNs for ovarian cancer treatment presents several limitations. (1) It exclusively examines SKOV3 ovarian cancer cells, potentially limiting the generalizability of the findings to other cell lines or cancer types. (2) The in vitro nature of the study may not accurately represent the complex interactions that would occur in vivo, leaving questions about the behavior of SAMNs within a living organism. (3) The concentration-dependent effects of alginate lyase are not thoroughly explored, leaving the optimal concentration for clinical application unclear. (4) The study's short-term focus, examining effects up to 3 days, does not provide insights into potential long-term effects or chronic toxicity. (5) While assessing cell membrane integrity, the study does not explore other potential side effects or systemic toxicities associated with SAMNs. (6) The absence of a comparative analysis with existing ovarian cancer therapies may limit understanding the relative effectiveness of this approach. (7) The lack of in-depth mechanistic insights into how SAMNs exert their effects could hinder the development of this therapeutic strategy. (8) Finally, potential challenges in scaling up the production of SAMNs for clinical use, including manufacturing, stability, and standardization issues, are not addressed. These limitations collectively highlight areas that require further investigation to fully understand the potential of SAMNs in ovarian cancer treatment.

Conclusions

In this study, we have successfully addressed the limitations associated with the use of alginate in nanoparticle formulations for delivering melittin, a potent anti-cancer agent with specific efficacy against ovarian cancer cells. Our innovative approach involved the integration of alginate lyase into SAMNs, which facilitated a more controlled and predictable release of melittin, enhancing its therapeutic efficacy while mitigating off-target effects. The JC-1 dye assay and Seahorse XF Analyzer results revealed that SAMNs, especially when combined with alginate lyase, significantly moderated the impact of melittin on mitochondrial membrane potential and cellular uptake in SKOV3 ovarian cancer cells. This was evident from the sustained high mitochondrial membrane potential in the control group and altered potential in groups treated with melittin and its encapsulated forms. Furthermore, the introduction of alginate lyase showed a dose-dependent effect

on cellular uptake and mitochondrial respiration, indicating an improved delivery mechanism for melittin. Our findings demonstrate that SAMNs extend the retention time of melittin, effectively control cell proliferation, and reduce the potential for unintended cellular damage. The inclusion of alginate lyase in the SAMNs formulation marks a significant advancement in the targeted treatment of ovarian cancer, offering a promising therapeutic strategy with reduced off-target cytotoxic effects.

Abbreviations

APTES	3-Aminopropyltriethoxysilane
CCCP	Carbonyl cyanide m-chlorophenyl hydrazone
CTAB	Cetyltrimethylammonium bromide
DLS	Dynamic light scattering
FBS	Fetal bovine serum
FCCP	Carbonyl cyanide-4-(trifluoromethoxy)phenylhydrazone
FTIR	Fourier-transform infrared spectroscopy
GAPDH	Glyceraldehyde-3-phosphate dehydrogenase
HPLC	High-performance liquid chromatography
LDH	Lactate dehydrogenase
MTT	3-(4,5-Dimethylthiazol-2-yl)- 2,5-diphenyltetrazolium bromide
OCR	Oxygen consumption rate
PBS	Phosphate-buffered saline
PVDF	Polyvinylidene difluoride
ROS	Reactive oxygen species
SAMNs	SiO2-alginate-melittin nano-conjugates
S.D.	Standard deviation
SDS-PAGE	SDS–polyacrylamide gel electrophoresis
SEM	Scanning Electron Microscopy
TEOS	Tetraethyl orthosilicate

Acknowledgements
This study was financially supported by The Science and Technology Department of Jilin Province (Grant No. YDZJ202201ZYTS580).

Author contributions
LS and YJ provided methodology, conducted the investigation, and wrote the draft. LS and RL carried out supervision, data analysis, conceptualization, and writing and editing. SY, SG and CY performed data analysis, software, and editing of the manuscript and YJ obtained the grant and supervised the project. All authors have read and endorsed the final manuscript.

Funding
This study was financially supported by The Science and Technology Department of Jilin Province (Grant No. YDZJ202201ZYTS580).

Availability of data and materials
All data generated or analyzed during this study are included in this article.

Declarations

Ethics approval and consent to participate
Not applicable.

Consent for publication
All the authors contributed to the article and approved the submitted version.

Competing interests
The authors declare that they have no known competing financial interests or personal relationships that could have appeared to influence the work reported in this paper.

Received: 26 September 2023 Accepted: 20 December 2023
Published online: 06 January 2024

References

Akbari R, Hakemi Vala M, Sabatier J-M, Pooshang Bagheri K (2022) Fast killing kinetics, significant therapeutic index, and high stability of melittin-derived antimicrobial peptide. Amino Acids 54:1275–1285

Akbarzadeh-Khiavi M, Torabi M, Olfati A-H, Rahbarnia L, Safary A (2022) Bio-nano scale modifications of melittin for improving therapeutic efficacy. Expert Opin Biol Ther 22:895–909
Alizadeh L, Alizadeh E, Zarebkohan A, Ahmadi E, Rahmati-Yamchi M, Salehi R (2020) AS1411 aptamer-functionalized chitosan-silica nanoparticles for targeted delivery of epigallocatechin gallate to the SKOV-3 ovarian cancer cell lines. J Nanopart Res 22:1–14
Ansari MO, Ahmad MF, Shadab G, Siddique HR (2018) Superparamagnetic iron oxide nanoparticles based cancer theranostics: a double edge sword to fight against cancer. J Drug Deliv Sci Technol 45:177–183
Babick F (2020) Dynamic light scattering (DLS). In: McNeil Scott E (ed) Characterization of nanoparticles. Elsevier, Amsterdam
Badr-Eldin SM, Alhakamy NA, Fahmy UA, Ahmed OAA, Asfour HZ, Althagafi AA, Aldawsari HM, Rizg WY, Mahdi WA, Alghaith AF et al (2020) Cytotoxic and pro-apoptotic effects of a sub-toxic concentration of fluvastatin on OVCAR3 ovarian cancer cells after its optimized formulation to melittin nano-conjugates. Front Pharmacol 11:642171
Badr-Eldin SM, Alhakamy NA, Fahmy UA, Ahmed OA, Asfour HZ, Althagafi AA, Aldawsari HM, Rizg WY, Mahdi WA, Alghaith AF (2021) Cytotoxic and pro-apoptotic effects of a sub-toxic concentration of fluvastatin on OVCAR3 ovarian cancer cells after its optimized formulation to melittin nano-conjugates. Front Pharmacol 11:642171
Bai X, Wang S, Yan X, Zhou H, Zhan J, Liu S, Sharma VK, Jiang G, Zhu H, Yan B (2020) Regulation of cell uptake and cytotoxicity by nanoparticle core under the controlled shape, size, and surface chemistries. ACS Nano 14:289–302
Bauersfeld SP, Kessler CS, Wischnewsky M, Jaensch A, Steckhan N, Stange R, Kunz B, Brückner B, Sehouli J, Michalsen A (2018) The effects of short-term fasting on quality of life and tolerance to chemotherapy in patients with breast and ovarian cancer: a randomized cross-over pilot study. BMC Cancer 18:1–10
Cheng X-Y, Biswas S, Li J, Mao C-J, Chechneva O, Chen J, Li K, Li J, Zhang J-R, Liu C-F (2020) Human iPSCs derived astrocytes rescue rotenone-induced mitochondrial dysfunction and dopaminergic neurodegeneration in vitro by donating functional mitochondria. Translational Neurodegeneration 9:1–14
Dai J, Cheng Y, Wu J, Wang Q, Wang W, Yang J, Zhao Z, Lou X, Xia F, Wang S (2020) Modular peptide probe for pre/intra/postoperative therapeutic to reduce recurrence in ovarian cancer. ACS Nano 14:14698–14714
Datta S, Barua R, Das J (2020) Importance of alginate bioink for 3D bioprinting in tissue engineering and regenerative medicine. In: Pereira Leonel (ed) Alginates—recent uses of this natural polymer. Intechopen, London
Harfmann D, Florea A (2023) Experimental envenomation with honeybee venom melittin and phospholipase A2 induced multiple ultrastructural changes in adrenocortical mitochondria. Toxicon 229:107136
Hui Y, Yi X, Wibowo D, Yang G, Middelberg APJ, Gao H, Zhao CX (2020) Nanoparticle elasticity regulates phagocytosis and cancer cell uptake. Sci Adv 6:4316
Keaswejjareansuk W, Keawmaloon S, Sawangrat N, Puttipipatkhachorn S, Yata T, Maitarad P, Shi L, Khongkow M, Namdee K (2021) Degradable alginate hydrogel microfiber for cell-encapsulation based on alginate lyase loaded nanoparticles. Mater Today Commun 28:102701
Khailova LS, Vygodina TV, Lomakina GY, Kotova EA, Antonenko YN (2020) Bicarbonate suppresses mitochondrial membrane depolarization induced by conventional uncouplers. Biochem Biophys Res Commun 530:29–34
Kuroki L, Guntupalli SR (2020) Treatment of epithelial ovarian cancer. BMJ. https://doi.org/10.1136/bmj.m3773
Mazibuko-Mbeje SE, Mthembu SX, Dludla PV, Madoroba E, Chellan N, Kappo AP, Muller CJ (2021) Antimycin A-induced mitochondrial dysfunction is consistent with impaired insulin signaling in cultured skeletal muscle cells. Toxicol Vitro 76:105224
Mir Hassani Z, Nabiuni M, Parivar K, Abdirad S, Karimzadeh L (2021) Melittin inhibits the expression of key genes involved in tumor microenvironment formation by suppressing HIF-1alpha signaling in breast cancer cells. Med Oncol 38:77
Nakamura H, Takada K (2021) Reactive oxygen species in cancer: current findings and future directions. Cancer Sci 112:3945–3952
Okon IS, Zou M-H (2015) Mitochondrial ROS and cancer drug resistance: implications for therapy. Pharmacol Res 100:170–174
Ouyang B, Poon W, Zhang Y-N, Lin ZP, Kingston BR, Tavares AJ, Zhang Y, Chen J, Valic MS, Syed AM (2020) The dose threshold for nanoparticle tumour delivery. Nat Mater 19:1362–1371
Perillo B, Di Donato M, Pezone A, Di Zazzo E, Giovannelli P, Galasso G, Castoria G, Migliaccio A (2020) ROS in cancer therapy: the bright side of the moon. Exp Mol Med 52:192–203
Pokhriyal R, Hariprasad R, Kumar L, Hariprasad G (2019) Chemotherapy resistance in advanced ovarian cancer patients. Biomarkers Cancer. https://doi.org/10.1177/1179299X19860815
Pulikkot S, Zhao M, Fan Z (2023) Real-time measurement of the mitochondrial bioenergetic profile of neutrophils. JoVE J Visuali Exp. https://doi.org/10.3791/64971
Qi J, Chen Y, Xue T, Lin Y, Huang S, Cao S, Wang X, Su Y, Lin Z (2019) Graphene oxide-based magnetic nanocomposites for the delivery of melittin to cervical cancer HeLa cells. Nanotechnology 31:065102
Ratajczak K, Lukasiak A, Grel H, Dworakowska B, Jakiela S, Stobiecka M (2019) Monitoring of dynamic ATP level changes by oligomycin-modulated ATP synthase inhibition in SW480 cancer cells using fluorescent "On-Off" switching DNA aptamer. Anal Bioanal Chem 411:6899–6911
Sangboonruang S, Kitidee K, Chantawannakul P, Tragoolpua K, Tragoolpua Y (2020) Melittin from apis florea venom as a promising therapeutic agent for skin cancer treatment. Antibiotics. https://doi.org/10.3390/antibiotics9080517
Severino P, da Silva CF, Andrade LN, de Lima OD, Campos J, Souto EB (2019) Alginate nanoparticles for drug delivery and targeting. Curr Pharm Des 25:1312–1334
Sivandzade F, Bhalerao A, Cucullo L (2019) Analysis of the mitochondrial membrane potential using the cationic JC-1 dye as a sensitive fluorescent probe. Bio-Protoc 9:e3128–e3128
Sopha P, Meerod T, Chantrathonkul B, Phutubtim N, Cyr DM, Govitrapong P (2023) Novel functions of the ER-located Hsp40s DNAJB12 and DNAJB14 on proteins at the outer mitochondrial membrane under stress mediated by CCCP. Mol Cell Biochem. https://doi.org/10.1007/s11010-023-04866-1
Sorasitthiyanukarn FN, Muangnoi C, Rojsitthisak P, Rojsitthisak P (2022) Chitosan oligosaccharide/alginate nanoparticles as an effective carrier for astaxanthin with improving stability, in vitro oral bioaccessibility, and bioavailability. Food Hydrocoll 124:107246

Sperling JA, Sakamuri SS, Albuck AL, Sure VN, Evans WR, Peterson NR, Rutkai I, Mostany R, Satou R, Katakam PV (2019) Measuring respiration in isolated murine brain mitochondria: implications for mechanistic stroke studies. NeuroMol Med 21:493–504
Sreenivasan PK, Kakarla VVP, Sharda S, Setty Y (2021) The effects of a novel herbal toothpaste on salivary lactate dehydrogenase as a measure of cellular integrity. Clin Oral Invest 25:3021–3030
Wang Y, Qi H, Liu Y, Duan C, Liu X, Xia T, Chen D, Piao H-l, Liu H-X (2021) The double-edged roles of ROS in cancer prevention and therapy. Theranostics 11:4839
Zheng M, Han B, Yang Y, Liu W (2011) Synthesis, characterization and biological safety of O-carboxymethyl chitosan used to treat Sarcoma 180 tumor. Carbohyd Polym 86:231–238
Zhou J, Wan C, Cheng J, Huang H, Lovell JF, Jin H (2021) Delivery strategies for melittin-based cancer therapy. ACS Appl Mater Interfaces 13:17158–17173

Publisher's Note